JUSTC

Article

http://justc.ustc.edu.cn

Descriptor for metal complex stability: synergistic effects of support, metal, and environmental conditions

Xu-Ting Chai[1], Mengru Li[1], Li Feng[1], Jin-Xun Liu[1,2], and Wei-Xue Li[1,2] ✉

[1]*State Key Laboratory of Precision and Intelligent Chemistry, University of Science and Technology of China, Hefei 230026, China;*
[2]*Hefei National Laboratory, University of Science and Technology of China, Hefei 230088, China*

✉Correspondence: Wei-Xue Li, E-mail: wxli70@ustc.edu.cn

Graphical abstract

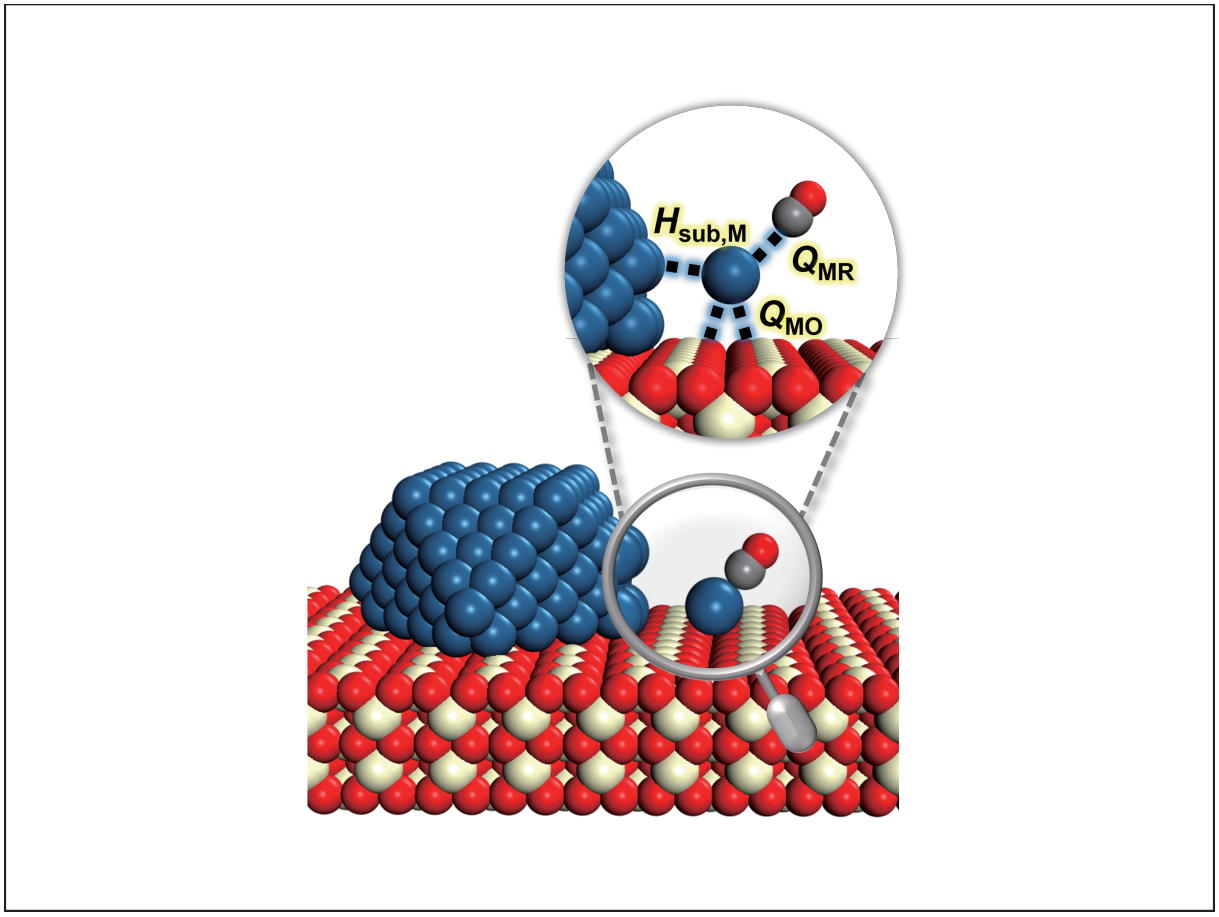

Public summary

-
-
-
-
-

Citation: Chai X T, Li M R, Feng L, et al. Descriptor for metal complex stability: synergistic effects of support, metal, and environmental conditions. *JUSTC*, **2026**, 55(0): . CSTR: 32290.14.JUSTC-2025-0010. DOI: 10.52396/JUSTC-2025-0010

JUSTC

Article

http://justc.ustc.edu.cn

Descriptor for metal complex stability: synergistic effects of support, metal, and environmental conditions

Xu-Ting Chai[1], Mengru Li[1], Li Feng[1], Jin-Xun Liu[1,2], and Wei-Xue Li[1,2] ✉

[1]*State Key Laboratory of Precision and Intelligent Chemistry, University of Science and Technology of China, Hefei 230026, China;*
[2]*Hefei National Laboratory, University of Science and Technology of China, Hefei 230088, China*

✉Correspondence: Wei-Xue Li, E-mail: wxli70@ustc.edu.cn

Cite This: *JUSTC*, **2026**, 55(X): (14pp) Read Online SI Supporting Information

Abstract: Transition metal catalysts supported on oxides undergo significant structural changes under reaction conditions, which are influenced by interactions with reactants. These interactions can lead to the dispersion of metal atoms, leading to the formation of stable single-nucleus metal complexes. Understanding the stability of these complexes is essential for catalyst design. In this study, we use multitask symbolic regression to identify a descriptor for the stability of single-nucleus metal complexes with common reactants, such as CO and H_2O, on the basis of first-principles calculations. We develop a multidimensional descriptor incorporating metal–metal, metal–support, and metal–adsorbate interactions, achieving high accuracy in predicting the stability of single-nucleus metal complexes. Our analysis revealed that in the absence of reactants, the stability of single metal atoms is mainly determined by the hardness (cohesive energy) of the metal. The presence of reactants such as CO and H_2O further stabilizes single-nucleus metal complexes by saturating undercoordinated metal atoms. This stabilization is correlated with the Lewis acidity of the surface oxygen in the support. Supports with lower Lewis acidity enhance metal–support interactions, promoting CO adsorption on all metals and H_2O adsorption on complexes of hard metals. In contrast, supports with higher Lewis acidity enhance hydrogen adsorption, promoting H_2O interactions with complexes of soft metals as well as Pd and Pt. Additionally, our descriptor predicts nanoparticle (NP) dissociation into single-nucleus metal complexes or Ostwald ripening (OR) tendencies. Under CO conditions, harder metals tend to favor dissociation, whereas softer metals (e.g., Ag, Cu, and Au) are more prone to OR. Under H_2O conditions, the Lewis acidity of the support surface oxygen influences NP behavior, with supports such as CeO_2 stabilizing single-nucleus metal complexes and promoting NP dissociation. These insights provide guidance for selecting catalyst components and optimizing reaction conditions to control the stability of single-nucleus metal complexes and guide NP dissociation or OR processes.

Keywords: single-nucleus complex; descriptor; multitask symbolic regression; first-principle calculation

CLC number: **Document code:** A

1 Introduction

Supported transition metal catalysts are essential in a variety of catalytic processes, such as ethanol steam reforming[1] and methane steam reforming[2]. The catalytic performance of these materials is significantly influenced by dynamic structural and compositional changes that occur under experimental conditions[3–5]. Metal nanoparticles can undergo transformations, including sintering or dispersion, leading to the formation of different active species, such as nanoparticles, clusters, and single atoms. Additionally, dispersed metal atoms can interact with reactants, resulting in the formation of single- or multinucleus metal complexes. Although these complexes are typically stable only under specific reaction conditions, the detection of metal complexes remains challenging because of their small size, dispersed nature, and uneven distribution, and advanced experimental and theoretical techniques are needed to distinguish them from other molecular species[6].

While single-atom metal catalysts (SACs) have garnered significant attention for their exceptional catalytic activity, there is limited research on the stability and reactivity of single-nucleus metal complexes, which may represent the true active species under reaction conditions. For example, Lu et al. identified $Pt(O)_3$ and $Pt(O)_4$ complexes during CO oxidation via operando EXAFS and DRIFTS[7]. Similarly, Yan et al.[8] investigated the structural dynamics of rhodium supported on CeO_2, revealing a transition from nanoparticles to $Rh_3(CO)_3$ complexes during methane steam reforming through in situ/operando characterization and first-principles modeling. Wu et al.[9] detected $Rh_1(OH)_1CO$ complexes during CO adsorption via in situ CO-DRIFTS and associated these species with the high activity of the catalyst. These studies underscore the importance of metal complexes under reaction conditions, as such insights are essential for identifying actual active configurations and designing more efficient catalysts.

The stability of single-nucleus metal complexes is influenced by the interactions between the metal, support, and en-

CSTR: 32290.14.JUSTC-2025-0010
DOI: 10.52396/JUSTC-2025-0010
JUSTC, **2026**, 55(X):

vironmental adsorbates. Soft metals (such as Ag, Cu, and Au) with low cohesive energies are more likely to break metal–metal bonds and exhibit a greater tendency to disperse from nanoparticles than hard metals are. For example, nanoclusters can form on Cu(111) and Cu(100) surfaces with fewer step sites, whereas similar behavior is observed only on stepped Pt(557) and Pt(332) surfaces[10–12]. Additionally, the support plays a critical role by providing anchoring sites for metal atoms through metal–support interactions. For example, Dvořák et al.[13] identified monoatomic step edges on CeO_2(111) surfaces as sites that anchor single Pt atoms via a combination of photoelectron spectroscopy, scanning tunneling microscopy, and density functional theory (DFT) calculations. Ligands from reactants in the environment can further stabilize undercoordinated dispersed metal atoms, increasing their overall stability. Lu et al.[7] demonstrated that single Pt atoms are stabilized as $Pt(O)_4$ species at step edge sites on CeO_2(111). Nie et al.[14] and Gänzler et al.[3] investigated the redispersion of Pt in an oxidizing environment (e.g., O_2) on CeO_2 and highlighted the influence of redox conditions on the stability of dispersed Pt atoms. Additionally, researchers have shown that hydroxyl groups from dissociated water facilitate the dispersion of metal atoms on the support, as demonstrated for the metals Ag[15], Cu[16], Pd[17], and Pt[18]. Therefore, the stability of metal complexes arises from a synergistic interplay among the hardness of the metal, the metal–support interactions, and the interactions between adsorbates and metal atoms.

Given the critical role of these interactions, extensive research has investigated the stability of supported SACs, with most studies attributing their resistance to aggregation to the binding energy of the metal atom on the support relative to the cohesive energy of the metal bulk[19–21]. Further studies have linked the binding energy to catalyst properties, such as the Fermi level of the metal atom and oxophilicity, as measured by the oxide formation energy, as well as support properties such as reducibility, as assessed via the oxygen vacancy formation energy[22,23]. Recently, our work[24] demonstrated that the oxophilicity of the supported metal and its affinity for the metal element in the oxide support serve as dominant descriptors for supported metal catalysts, including SACs. However, the identification of descriptors for the stability of metal complexes on supports under experimental conditions remains elusive, which hinders more efficient catalyst design with high stability and activity.

In this study, we used a data-driven machine learning technique, namely, multitask symbolic regression[25] with Sure Independence Screening and Sparsifying Operator (SISSO)[26,27], to identify the descriptors for predicting the formation energy of metal complexes on a support relative to their bulk metal phase, with a specific focus on single-nucleus metal complexes. A multidimensional descriptor was constructed by considering the interactions that govern the formation of single-nucleus metal complexes on a support. These interactions encompass the metal–metal interactions in the bulk metal phase, interactions between the single metal atoms and the support, and interactions between the adsorbates and the single metal atoms. The interaction between metal atoms in their bulk phase is represented by the enthalpy of sublimation of the bulk metal M, which corresponds to the negative cohesive energy at 0 K[28]. For the interaction between the metal and the support, a simplification was made by focusing on the interaction between the metal atom and the oxygen atoms of the support. This was quantified through the dissociation energy of a metal oxide phase. Finally, the interaction between the adsorbate and the metal atom is captured by the energy cost of dissociating the gas–phase metal–adsorbate complex. These three interaction terms were translated into simple features that collectively provide a systematic and accurate understanding of the formation energy of single-nucleus metal complexes on a support. This approach integrates thermodynamic principles and mathematical analysis to enable precise predictions while maintaining interpretability through physically meaningful descriptors.

2 Computational details

2.1 Methods

Spin-polarized periodic first-principles calculations were performed via density functional theory (DFT) within the Vienna ab initio simulation package (VASP)[29,30]. The generalized gradient approximation (GGA) with the Perdew–Burke–Ernzerhof (PBE) functional[31] was applied to account for exchange–correlation effects, whereas the projected-augmented wave (PAW)[32,33] method was employed to describe the interactions between the valence and core electrons. A kinetic energy cutoff of 400 eV was used for the plane wave basis set. To accurately describe the localized d states in metal atoms, the PBE + U approach[34] was employed with the $U - J$ parameter set to 3.0 eV[35–38] for the Ce, Zr, Hf, Ti and Th atoms.

The optimization of bulk lattice constants was performed via a 6×6×6 k-point mesh[39], with convergence achieved when the atomic forces dropped below 0.02 eV/Å. The optimized lattice constant was found to be 5.49 Å for CeO_2, which closely aligns with the experimental value of 5.41 Å[40]. A 2×2×1 k-point mesh was applied for the slab calculations, and the structures were considered converged when the forces on the atoms were reduced to less than 0.05 eV/Å. Dipole correction was implemented to reduce interactions between surface dipoles and their periodic counterparts, and a vacuum layer of 15 Å was introduced to prevent artificial interactions along the surface normal.

2.2 Models

The structures of the M_1/CeO_2, M_1/ZrO_2, M_1/HfO_2, M_1/TiO_2, and M_1/ThO_2 surfaces were constructed by positioning a single M atom on a three-layer (2×2) supercell of the (110) surfaces of the fluorite-type CeO_2, ZrO_2, HfO_2, TiO_2, and ThO_2 surfaces, respectively (Fig. 1). The set of metals (M) comprises late transition metals (Fe, Co, Ni, Cu, Ru, Rh, Pd, Ag, Os, Ir, Pt, and Au) and early transition metals (Ti, V, Cr, Mn, Zr, Nb, Mo, Hf, Ta, W, and Re). During geometry optimization, the bottom atomic layer of the supports was kept fixed, while the reactant molecules and the top two layers of the support were allowed to relax. For the supported metal atoms, relaxation is only allowed along the z-axis to ensure that the structure remains at the bridge oxygen site, which is

CSTR: 32290.14.JUSTC-2025-0010
DOI: 10.52396/JUSTC-2025-0010
JUSTC, **2026**, 55(X):

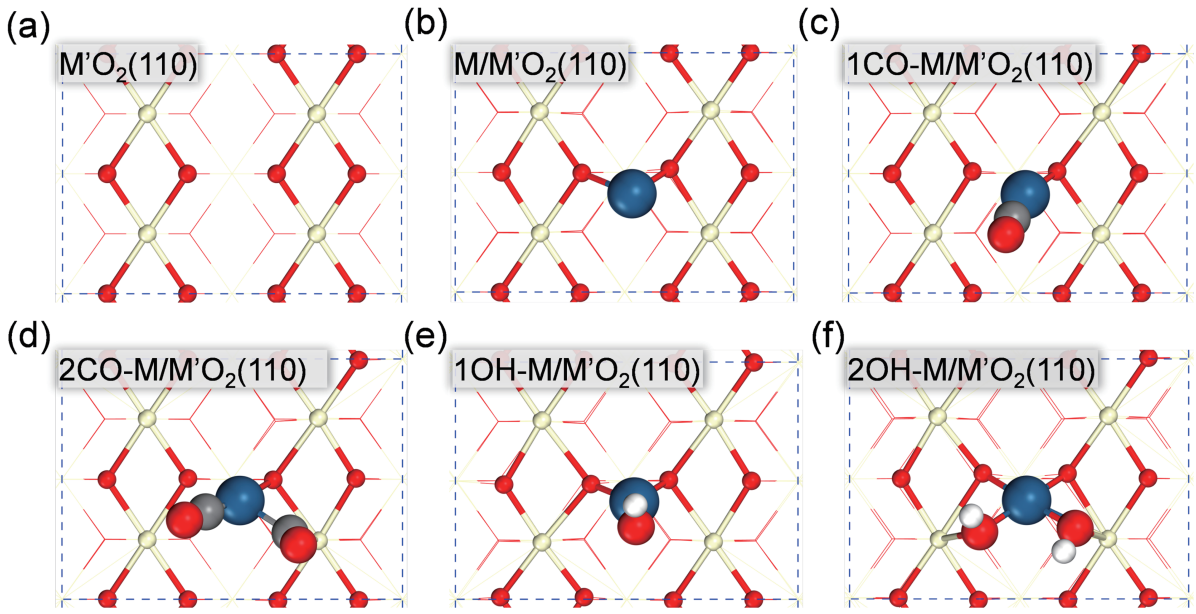

Fig. 1. (a) Top view of the stoichiometric M'O_2(110) (M' = Ce, Zr, Ti, Hf, and Th) surface. (b) Top view of a single metal atom (M) on the fluorite-type M'O_2(110) surface, denoted as M/M'O_2. (c–f) Configurations showing the adsorption of one CO molecule ('1CO') (c), two CO molecules ('2CO') (d), one OH group ('1OH') (e), and two OH groups ('2OH') (f) adsorbed at the M/CeO_2 surface. The dashed blue lines mark the boundary of the slab model's unit cell. Color coding: beige (Ce), blue (M), red (O), light gray (H). Only the atoms in the uppermost layer of the support and the Pt atom are depicted as solid circles, whereas those in the lower layers are represented by lines.

considered the optimal adsorption site[41,42].

To evaluate the stability of these complexes in the presence of reactants (CO or H_2O), we calculated the formation energy (E_f) with respect to the bulk M, support, and gaseous CO and H_2O as reference states:

$$E_f=(E_{tot}-E_{M1}-E_{slab}-x^*E_{CO}-y^*E_{H_2O})/(x+y) \quad (1)$$

where E_{tot}, E_{M1}, E_{slab}, E_{CO} and E_{H_2O} represent the electronic energies of the total system (including the catalyst and reactants, as for H_2O, the OH group binds to the supported metal atom, whereas the H atom attaches to a lattice oxygen at an infinite distance from the metal atom), a metal atom in the bulk phase, the support, and the reactants (CO and H_2O) in the gas phase, respectively, as calculated from DFT. E_f was averaged over each reactant molecule (with x and y representing the numbers of CO and H_2O, respectively).

Next, considering the experimental conditions such as the temperature and partial pressure of the reactants, we calculated the formation free energy (G_f) via the following equation:

$$G_f=E_f-\mu_{reactant} \quad (2)$$

where $\mu_{reactant}$ represents the chemical potential of gaseous CO or H_2O, which is dependent on temperature and partial pressure.

To characterize the E_f of single-nucleus metal complexes, three interaction components were considered: the cohesive energy of M in the bulk phase, represented as the negative of its enthalpy of sublimation ($-H_{sub,M}$)[28]; the interaction between the single metal atoms and the support (Q_{MO}); and the interaction between the single metal atoms and the reactants in the gas phase (Q_{MR}). First, the enthalpy of sublimation of metal M in its bulk phase, $H_{sub,M}$, is calculated via the following equation:

$$H_{sub,M}=E_M^{gas}-E_M^{bulk} \quad (3)$$

Here, E_M^{gas} and E_M^{bulk} denote the energies of a metal atom in the gas phase and the bulk phase, respectively. Next, the interaction between the M atom and the support is modeled by the interaction between the M atom and an oxygen atom since the M atom is positioned at the bridge site between adjacent lattice oxygen ions in the support. This is represented by the dissociation energy (Q_{MO}) of the most stable metal oxide phase, MO_x, into metal atoms and oxygen in the gas phase. The Q_{MO} is expressed by the following equation:

$$Q_{MO}=E_M^{gas}+\frac{x}{2}E_{O_2}^{gas}-E_{MO_x}^{bulk} \quad (4)$$

where $E_{O_2}^{gas}$ and $E_{MO_x}^{bulk}$ represent the energies of the oxygen molecules in the gas phase and one unit cell of the MO_x bulk phase, respectively. The value of x represents the ratio of oxygen atoms to M atoms in the bulk phase. Finally, the interaction between the reactant (CO or H_2O) and the metal atom M under experimental conditions (Q_{MR}) is evaluated by considering the energy cost for the decomposition of the complex (denoted by 'R-M') into the single metal atom M and the reactant R in the gas phase, as represented by the following equation:

$$Q_{MR}=E_M^{gas}+E_R^{gas}-E_{R\text{-}M}^{gas} \quad (5)$$

Here, E_R^{gas} and $E_{R\text{-}M}^{gas}$ are the energies of the metal complex R-M and reactant R in the gas phase, respectively.

3 Results and discussion

To identify effective descriptors for supported single-nucleus metal complexes, we first focused on developing a descriptor

CSTR: 32290.14.JUSTC-2025-0010
DOI: 10.52396/JUSTC-2025-0010
JUSTC, **2026**, 55(X):

for the stability of SACs in the absence of reactants. This multidimensional descriptor includes features that describe the interactions among the various components within the catalyst system. This initial analysis is based on DFT calculations of E_f for twelve single metal atoms (M), including Fe, Co, Ni, Cu, Ru, Rh, Pd, Ag, Os, Ir, Pt, and Au, supported on various four fluorite-type metal oxide supports, such as CeO_2, ZrO_2, TiO_2, and HfO_2. The descriptor was tested using data for SACs formed by early transition metal (M_{early}) species—namely, Ti, V, Cr, Mn, Zr, Nb, Mo, Hf, Ta, W, and Re—and by extending the analysis to a broader range of supports, including CeO_2, HfO_2, and ThO_2. Next, we incorporated common reactants such as CO or H_2O to explore the descriptor for the E_f of single-nucleus metal complexes under experimental conditions. Once this descriptor was identified and validated, we investigated how key factors—such as metal hardness, the oxygen affinity of the metal atom, and the reactant adsorption strength, which are integral components of the descriptor—impact the stability of these metal complexes. This exploration provides a comprehensive understanding of the factors governing the stability of supported single-nucleus metal complexes and the potential for Ostwald ripening (OR) and dissociation of NPs.

3.1 Descriptor for the SAC stability

To systematically investigate descriptors for the stability of SACs, we focused on key features related to the cohesive energy of the metal bulk phase and the interaction between the single metal atoms and the support. Previous studies[21,43] have established that stability is largely governed by the binding energy of metal atoms during the sintering process. Specifically, a higher cohesive energy promotes single metal atom aggregation, whereas stronger interactions between single metal atoms and supports stabilize undercoordinated metal atoms and enhance their dispersion. To quantify the cohesive energy of the metal bulk phase, we used the enthalpy of sublimation of the metal ($H_{sub,M}$) in its bulk phase. Additionally, we simplified the interaction between the metal atom and support by focusing on the interaction with oxygen, as the metal atom is typically adsorbed at the bridge site of lattice oxygen ions within the (110) surface of the fluorite-type support. This interaction is characterized by the dissociation energy of a corresponding metal oxide phase (Q_{MO}).

To determine how these features influence the stability of SACs, we employed multitask symbolic regression within the framework of the SISSO. The analysis was trained on a comprehensive dataset that includes the E_f of single metal atoms on the basis of DFT calculations. This dataset consists of twelve late transition metals—Fe, Co, Ni, Cu, Ru, Rh, Pd, Ag, Os, Ir, Pt, and Au—supported on four distinct oxide supports (CeO_2, ZrO_2, TiO_2, and HfO_2) (Fig. 2a). This training dataset includes data for a range of metals, spanning soft metals such as Ag, Cu, and Au to harder metals, and features a variety of supports, encompassing both support with stronger interactions with metal atoms (CeO_2, TiO_2) and support with weaker interactions (ZrO_2, HfO_2), as indicated by the normalized metal–support interaction (MSI) above and below 0.5, respectively[44] (Fig. S4). This approach allows for

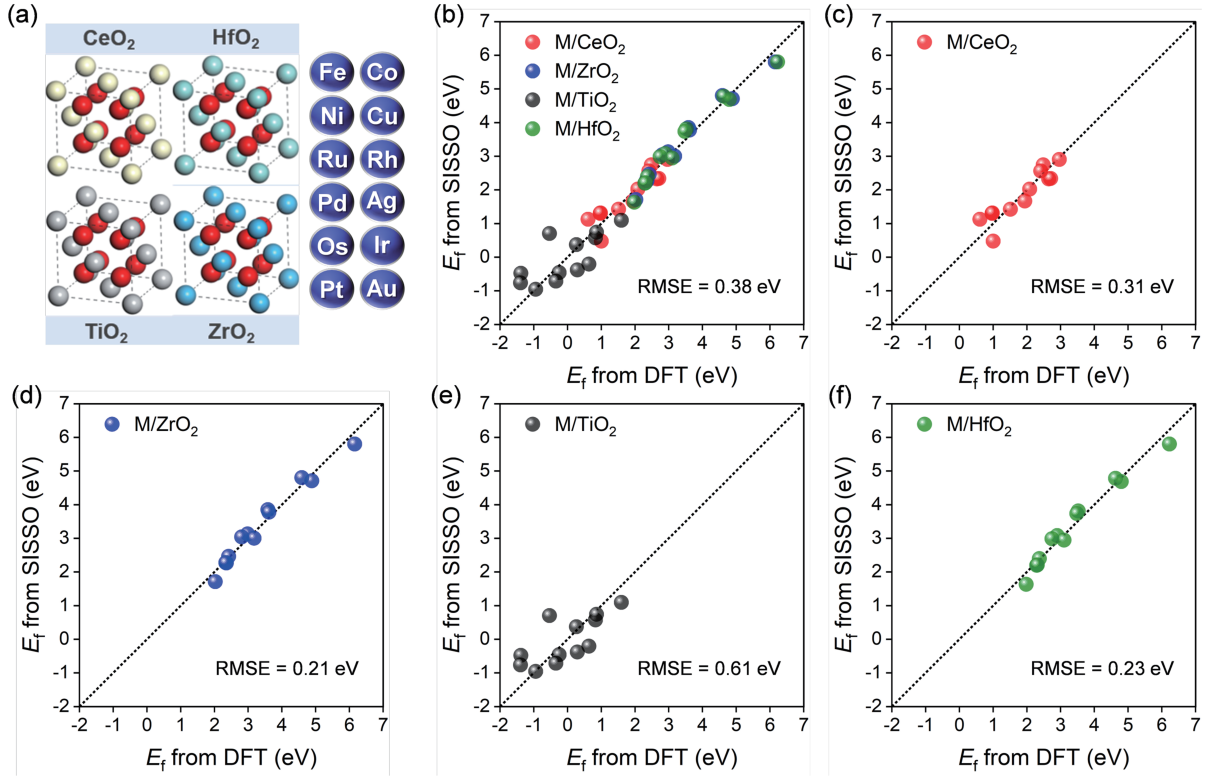

Fig. 2. (a) Schematic representation of the training dataset, including various late transition metals (M) and oxide supports. (b) Comparison of the formation energy (E_f) of single-atom catalysts (SACs) on CeO_2, ZrO_2, TiO_2, and HfO_2 supports, as calculated via DFT and as estimated via Eq. (6). Panels (c-f) present this relationship for SACs supported individually on CeO_2 (c), ZrO_2 (d), TiO_2 (e), and HfO_2 (f).

CSTR: 32290.14.JUSTC-2025-0010
DOI: 10.52396/JUSTC-2025-0010
JUSTC, **2026**, 55(X):

a systematic exploration of how these selected features contribute to the stability of single metal atoms on various supports.

After exploring various dimensions and feature complexities, we identified a simple and interpretable functional form that achieves high accuracy, with an RMSE of 0.38 eV—compared with the typical data noise in DFT calculations. The same regression functional form is used across all the supports, represented by the sum of $H_{sub,M}$ and the Q_{MO} weighted by their respective coefficients, as shown in the equation below:

$$E_f = c_1 H_{sub,M} + c_2 Q_{MO} + c_0 \quad (6)$$

Here, c_1 is positive, whereas c_2 is negative or positive, and both vary depending on the specific support, ranging from CeO_2 (red dots), ZrO_2 (blue dots), and TiO_2 (black dots) to HfO_2 (green dots), as shown in Fig. 2b. $H_{sub,M}$ and the Q_{MO} were selected as key features in this study because of their ability to capture essential catalytic behavior, ensuring that the model remains simple, interpretable, and accessible for analysis. A larger c_1 reflects a greater degree of metal–metal interactions on the support, promoting aggregation. Conversely, a more negative c_2 reflects a stronger interaction between the metal atom and the support, which counteracts aggregation and stabilizes dispersion. Since the most stable metal oxide was selected as the reference to obtain the Q_{MO}, the bond strength for this reference may exceed the interaction energy between the metal atom and lattice oxygen in supports, such as ZrO_2 and HfO_2 with weaker metal–oxygen interactions (Fig. S4). Consequently, this choice can overestimate the Q_{MO}, resulting in positive c_2 values. However, this does not affect the functional form of the descriptor.

First, we observed that across all the supports, the c_1 values are greater than the absolute values of c_2, highlighting the dominant influence of the metal cohesive energy over the metal–support interactions. Second, the c_1 values for different supports follow the trend of $CeO_2 > TiO_2 > HfO_2 \approx ZrO_2$. Similarly, the c_2 value is also highest for CeO_2, followed by TiO_2, while the values for HfO_2 and ZrO_2 are approximately zero (Table 1). These results suggest that only supports with strong interactions with metals, such as CeO_2 and TiO_2, significantly influence the stability of SACs, with CeO_2 emerging as the most effective support for SAC design.

We further analyzed the data by separating it on the basis of different supports to evaluate the robustness and reliability of the descriptor. The subsets shown in Fig. 2c–f span distinct energy ranges with varying degrees of scatter. The corresponding training RMSE values are 0.31, 0.21, 0.61, and 0.23 eV, respectively. These results demonstrate that this two-dimensional descriptor is applicable across a wide range of SACs. The relatively high RMSE for SACs on TiO_2 arises from the data point for Pt_1, which shows the largest positive deviation from the DFT-calculated E_f. This deviation may be attributed to structural deformation reflected by the notable upshift of the two lattice oxygen atoms coordinated to the Pt atom. Notably, the data points for ZrO_2 and HfO_2 overlap in Fig. 2b at more positive E_f values, indicating the comparable and relatively lower stability of SACs than that of CeO_2 and TiO_2. This trend aligns with the weaker influence of both metal–support interactions and cohesive energy on complex stability, as indicated by the smaller absolute values of c_2 and c_1, respectively (Table 1).

To further validate the generalizability of Eq. (6), we conducted systematic modifications on the catalysts in the test set (Fig. 3a). First, we varied the metal, replacing late transition metals (M) with early transition metals (mainly Ti, V, Cr, Mn, Zr, Nb, Mo, Hf, Ta, W, and Re) on CeO_2 (red circles in Fig. 3b) and HfO_2 (green circles in Fig. 3b). This subset is denoted by Test-1. Next, we substituted the supports with ThO_2 while keeping the late transition metals M unchanged (denoted by the Test-2 subset in Fig. 3a and the orange dots in Fig. 3b). Finally, we simultaneously modified both the metal and support, replacing late transition metals with early transition metals and the support with ThO_2 (denoted by the Test-3 subset in Fig. 3a and denoted by orange circles in Fig. 3b). These modified catalysts are distinct from the original systems in the training set.

Fig. 3b compares the E_f values for the test set predicted by Eq. (6) with those calculated via DFT, showing an RMSE of 0.35 eV, which is slightly lower than the RMSE for the training set. This underscores the robust generalizability of Eq. (6). Similar to M on the supports in the training set, the c_1 values are significantly greater than the absolute values of c_2 for the test set, indicating that the cohesive energy of the metal can effectively estimate the feasibility of SAC formation. We categorized the data points into four subsets for M_{early}/CeO_2, M_{early}/HfO_2, M/ThO_2, and M_{early}/ThO_2, achieving RMSE values of 0.30, 0.55, 0.23, and 0.21 eV, respectively. Fig. 3c–f il-

Table 1. Coefficients and RMSEs of the functional derived from multitask symbolic regression for E_f of single metal atoms in the training and test sets without reactants.

System		c_1 ($H_{sub,M}$)	c_2 (Q_{MO})	c_0	RMSE (eV)
Training Set	M/CeO_2	0.98	−0.42	−0.16	0.31
	M/ZrO_2	0.58	0.12	−0.35	0.21
	M/TiO_2	0.75	−0.23	−2.20	0.61
	M/HfO_2	0.59	0.12	−0.47	0.23
Test Set	M_{early}/CeO_2	1.19	−0.56	1.53	0.30
	M_{early}/HfO_2	1.46	−0.62	3.20	0.55
	M_{early}/ThO_2	1.35	−0.44	1.68	0.23
	M/ThO_2	0.59	0.14	−0.76	0.21

CSTR: 32290.14.JUSTC-2025-0010
DOI: 10.52396/JUSTC-2025-0010
JUSTC, **2026**, 55(X):

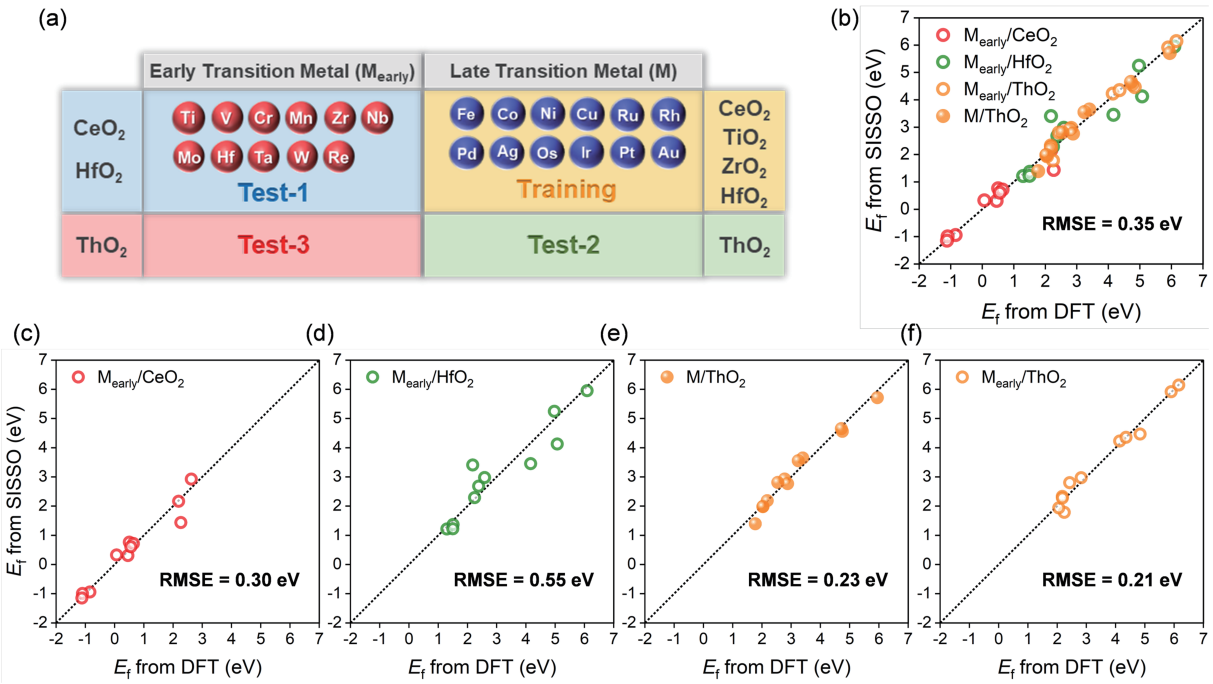

Fig. 3. (a) Schematic representation of the training and test datasets, including various late transition metals (M), early transition metals (M_{early}) and oxide supports. (b) Comparison of the formation energies of single-atom catalysts (SACs) on CeO_2, HfO_2, and ThO_2, as calculated via DFT and as estimated via Eq. (6). Panels (c–f) present this relationship for SACs composed of M_{early} supported individually on CeO_2 (c), HfO_2 (d), ThO_2 (f), and M supported on ThO_2 (e).

lustrates these subsets, which cover distinct energy ranges and exhibit varying levels of scatter. These findings highlight the broad applicability of this two-dimensional descriptor to diverse supported metal catalysts.

For CeO_2, HfO_2, and ThO_2, the c_1 and absolute values of c_2 for supported M_{early} are greater than those for M (Table 1), reflecting the greater influence of metal hardness and metal–support interactions. The significantly higher $H_{sub,M}$ and Q_{MO} for M_{early} than for M correspond to a more pronounced variation in E_f (Table S1). Thus, the stability of SACs formed by M_{early} on supports can vary more significantly with changes in metal species.

3.2 Descriptor for single-nucleus complex stability

Building upon the exploration of descriptors for SAC stability, we extended our investigation to examine the formation energy of single-nucleus metal complexes in the presence of common industrial reactants, CO and H_2O, as shown in Fig. 4a. For H_2O, which readily dissociates into OH and H on SACs, we focused primarily on its dissociated form. In this configuration, the OH group binds to the supported metal atom, whereas the H atom attaches to a lattice oxygen at an infinite distance from the metal atom. To account for the interaction between the metal atom and the adsorbate, we introduced an additional feature—the dissociation energy of the single-nucleus complex in the gas phase (Q_{MR}). We utilized multitask symbolic regression to derive a concise and interpretable functional form for the descriptor of E_f for single-nucleus metal complexes. The catalyst systems in the training dataset for the metal complexes are the same as those used in the training dataset for the SACs, as depicted in Fig. 2a, with CO and dissociated H_2O as reactants. To investigate the influ-

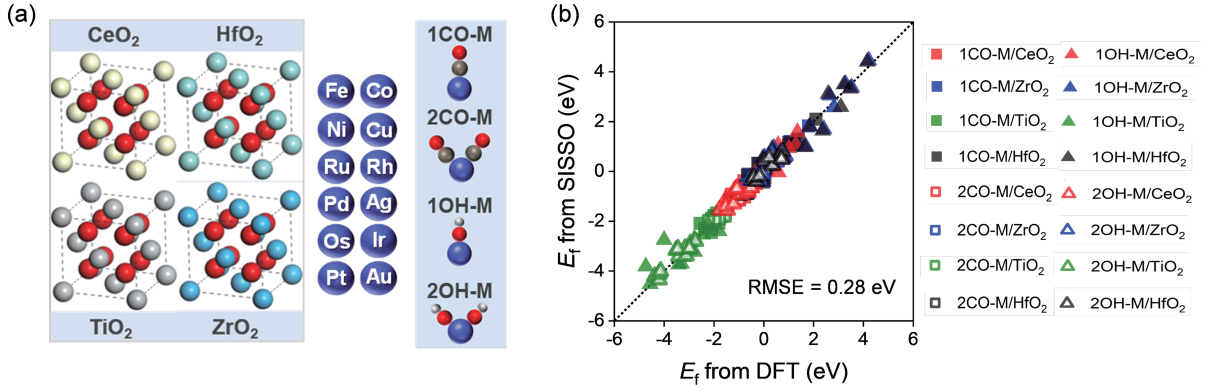

Fig. 4. (a) Schematic representation of the training dataset, including various late transition metals (M), oxide supports, and reactants. (b) Comparison of the formation energies of single-nucleus metal complexes on CeO_2, ZrO_2, TiO_2, and HfO_2 supports the presence of 1 CO molecule ('1CO'), 2 CO molecules ('2CO'), 1 dissociated H_2O molecule ('1OH'), and 2 dissociated H_2O molecules ('2OH'), as calculated via DFT and predicted by Eq. (7).

CSTR: 32290.14.JUSTC-2025-0010
DOI: 10.52396/JUSTC-2025-0010
JUSTC, **2026**, 55(X):

ence of pressure on the stability of single-nucleus metal complexes, we adjusted the number of reactant molecules: a single molecule (labeled '1CO' and '1OH', indicated by the filled square and triangle symbols in Fig. 4b) and two molecules (labeled '2CO' and '2OH', indicated by the empty square and triangle symbols in Fig. 4b) within the single-nucleus metal complexes. We used the test set for SACs as catalyst systems, incorporating '1CO', '2CO', '1OH', and '2OH' into the test set, as shown in Fig. 6a.

Consequently, for the training dataset shown in Fig. 4a, the Q_{MR} was integrated into the descriptor for the E_f of SACs, and the E_f of single-nucleus metal complexes becomes a function of $H_{sub,m}$, Q_{MO}, and Q_{MR} with a low RMSE of 0.28 eV, as represented in the equation below:

$$E_f = c_1 H_{sub,M} + c_2 Q_{MO} + c_3 Q_{MR} + c_0 \quad (7)$$

Here, as shown in Table S4, c_1 is positive, and c_2 is approximately zero, indicating that the metal–oxygen interaction has a negligible effect on systems with identical support and reaction conditions. c_3 is negative, and a more positive Q_{MR} suggests stronger attracting interactions between the reactants and the single metal atom in the gas phase, enhancing the stability of the single-nucleus metal complexes and leading to a more negative E_f. Both c_1 and c_3 are comparable and significantly greater than c_2, as shown in Table S4, indicating a similar influence from the metal hardness and the adsorption of reactants. The coefficients change depending on the type of reactant species and the support.

Fig. 4b presents a comparison between the E_f values calculated from Eq. (7) and those obtained from DFT calculations for systems in the training set (Fig. 4a), with a low RMSE of 0.28 eV, demonstrating the accuracy of Eq. (7) in describing E_f. We subsequently categorized the data points on the basis of the presence of specific reactants, as shown in Fig. 5: '1CO'

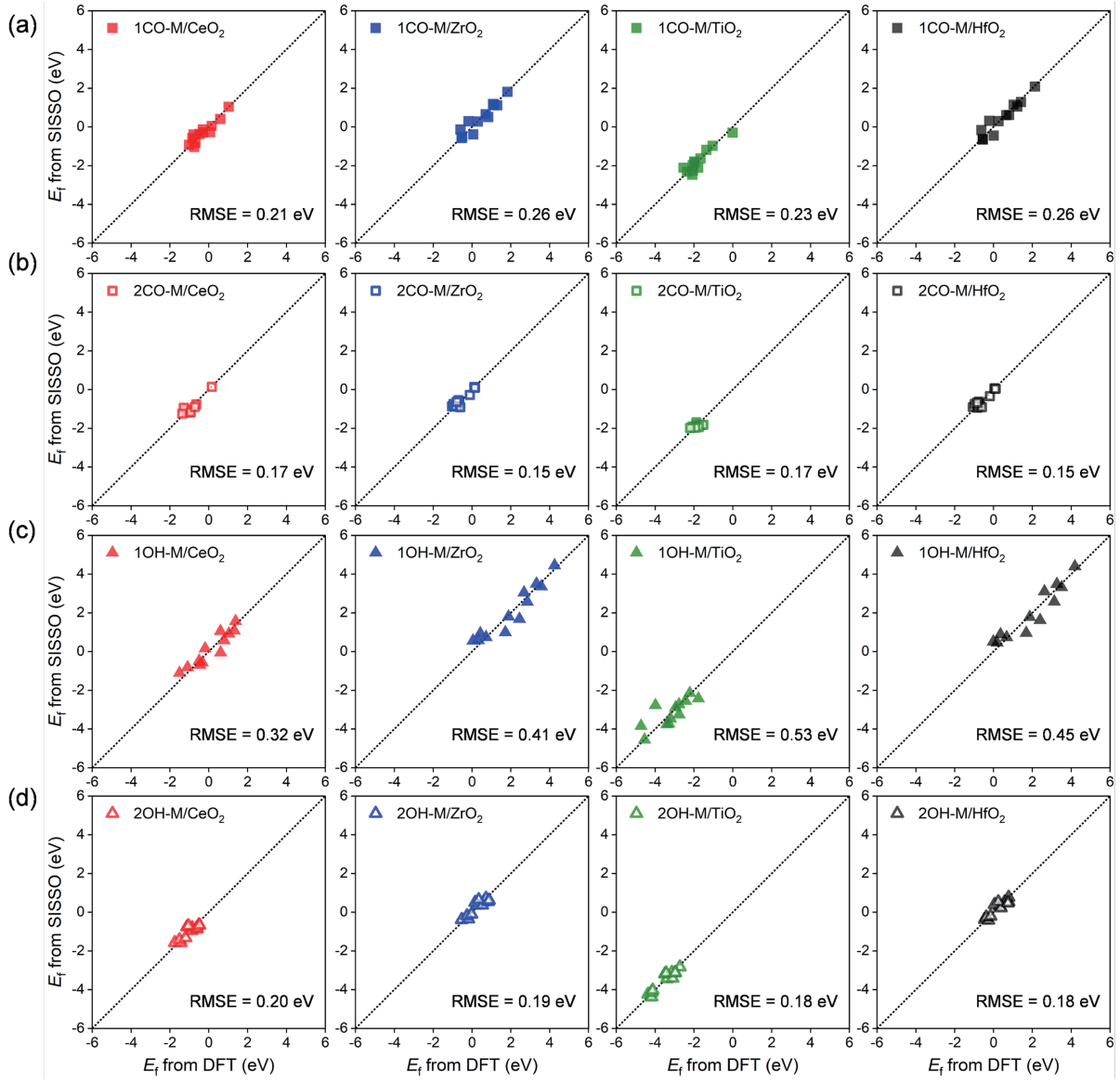

Fig. 5. Comparison of the formation energies of single-nucleus metal complexes on CeO_2 (a), ZrO_2 (b), TiO_2 (c), and HfO_2 (d) support in the presence of 1 CO molecule ('1CO'), 2 CO molecules ('2CO'), 1 dissociated H_2O molecule ('1OH'), and 2 dissociated H_2O molecules ('2OH'), as calculated via DFT and predicted by Eq. (7).

CSTR: 32290.14.JUSTC-2025-0010
DOI: 10.52396/JUSTC-2025-0010
JUSTC, **2026**, 55(X):

(Panel a), '2CO' (Panel b), '1OH' (Panel c), and '2OH' (Panel d). For each reactant, the data were further divided by support type—CeO_2, ZrO_2, TiO_2, and HfO_2—displayed in panels from left to right with low RMSEs ranging from 0.15 eV to 0.26 eV, except in cases involving the presence of '1OH'. The largest RMSE for systems with '1OH', ranging from 0.32 eV to 0.53 eV, may be attributed to the binding of OH to both the single metal atom and the metal ion in the support. The interaction between OH and the metal ion in the support, however, is not captured by Eq. (7). Fig. 5 shows that the range of E_f varies with changes in both reactants and supports, and the distribution of points differs across the panels. These observations confirm that the proposed functional form is applicable and can be extended to a broad range of single-nucleus complex systems.

To further evaluate the generalizability of Eq. (7), we conducted a series of tests using the transferability dataset, as shown in Fig. 6a. This allowed us to assess how well Eq. (7) performs when it is applied to different catalyst systems. The calculated E_f values from both Eq. (7) and DFT show good agreement, with lower RMSE values of 0.27, 0.21, and 0.16 eV, as illustrated in Fig. 6b, c, and d, respectively. The coefficients c_1, c_2, and c_3 vary with respect to changes in reactants and supports (Table S4).

For the test dataset, the c_2 values are approximately zero, whereas the c_1 values are positive and the c_3 values are negative, which is consistent with the results in the training dataset for the complexes. Notably, the absolute values of c_1 and c_3 are comparable, contributing similarly to E_f. This suggests that the hardness of the metal and the impact of reactant adsorption are consistently the dominant factors influencing the stability of single-nucleus metal complexes on the same support under identical reaction conditions. These findings demonstrate that changes in the metal species affect E_f primarily through variations in the metal hardness and metal–adsorbate interactions.

Furthermore, we evaluated the regression function on two additional comprehensive datasets. First, to assess the impact of U correction on the regression functional, we selected systems consisting of CeO_2 and 12 metals in the presence of '1CO', '2CO', '1OH', and '2OH' from the training set in Fig. 6a, adopting a different U value of 5 eV for the d-orbitals of Ce. As shown in Fig. S1a, a strong consistency was observed between the E_f values from the DFT calculations and those predicted by Eq. (7), with an RMSE of 0.22 eV. This result indicates that the generalizability of Eq. (7) is unaffected by the value of the U correction.

Additionally, we tested a second dataset comprising E_f values of complexes formed by these metals on the (110) surface of rutile-type TiO_2, as reported in a previous study[45]. Unlike our original dataset, which focused on fluorite-type MO_2 supports, this dataset provided a distinct comparison. Remarkably, Eq. (7) demonstrated robust accuracy for predicting E_f, achieving an RMSE of 0.19 eV (Fig. S1b). Therefore, although the calculation parameters of E_f and the crystal phase of oxides are different, the multidimensional descriptor, represented by the combined interactions of the system components, can serve as a universal descriptor for assessing the

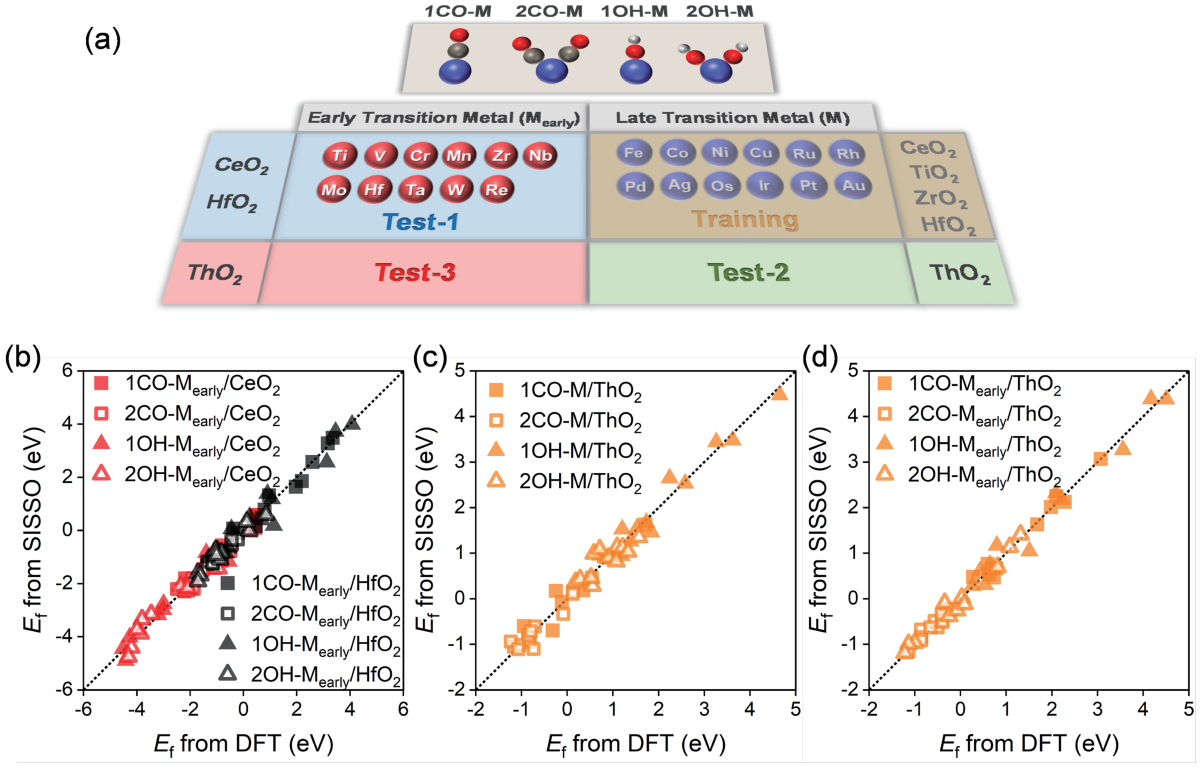

Fig. 6. (a) Schematic representation of the training and test datasets, including various late transition metals (M), early transition metals (M_{early}) and oxide supports. (b) Comparison of the formation energies of single-nucleus metal complexes involving M_{early} on CeO_2, as calculated via DFT and predicted via Eq. (7). (c) The same comparison for single-nucleus metal complexes involving M on ThO_2. (d) Comparison of the formation energy for M_{early} on ThO_2, calculated via DFT and estimated via Eq. (7).

CSTR: 32290.14.JUSTC-2025-0010
DOI: 10.52396/JUSTC-2025-0010
JUSTC, **2026**, 55(X):

stability of single-nucleus metal complexes.

3.3 Influence of catalyst components and reaction conditions on stability

Following the investigation of the descriptors for single-nucleus metal complexes, we next examined the impact of catalyst properties and reaction conditions on the stability of single-nucleus metal complexes. This analysis incorporates factors associated with the features from Eq. (7), including the metal hardness, the oxygen affinity of the metal atom, the Lewis acidity of the lattice oxygen in the support, and the presence of H_2O or CO.

3.3.1 Impact of metal hardness

As shown in Eq. (7), E_f for a single-nucleus complex is related to the hardness of the metal reflected by a larger $H_{sub,M}$. A stronger interaction between metal atoms in the bulk makes E_f more positive, indicating less stability of the corresponding single-nucleus metal complexes. To explore the relationship between the hardness of metal M and the stability of single-nucleus metal complexes, we first focused on SACs in the absence of reactants. The E_f values for SACs formed by metals ranging from soft (e.g., Ag, Cu, and Au) to hard (e.g., Pd, Fe, Co, Ni, Rh, Pt, Ru, Ir, and Os) metals were calculated on ZrO_2 and CeO_2 supports via Eq. (6), as shown in Fig. 7a. ZrO_2 and CeO_2 exemplify two types of supports characterized by weaker and stronger interactions with metal atoms, respectively. These E_f values are approximately consistent with those derived from DFT calculations (Fig. S2). Fig. 7a indicates that all E_f values are positive, confirming the instability of the SACs. On ZrO_2, E_f becomes more positive as the metal hardness increases from left to right, reflecting the dominant influence of cohesive energy on SAC stability. This is consistent with the larger value of c_1, whereas the c_2 values for ZrO_2 are approximately zero (Table 1). In contrast, the E_f values of CeO_2 do not clearly depend on the cohesive energy, suggesting the combined impact of both the metal's cohesive energy and its interaction with the support.

3.3.2 Impact of oxygen affinity

Following the investigation of the relationship between metal hardness and the stability of SACs, we next focused on the interaction between the metal atom and the support. This interaction is represented by the Q_{MO}, which also reflects the oxygen affinity of the metal atom. As discussed above, compared with ZrO_2, Q_{MO} has a greater effect on E_f on CeO_2. To

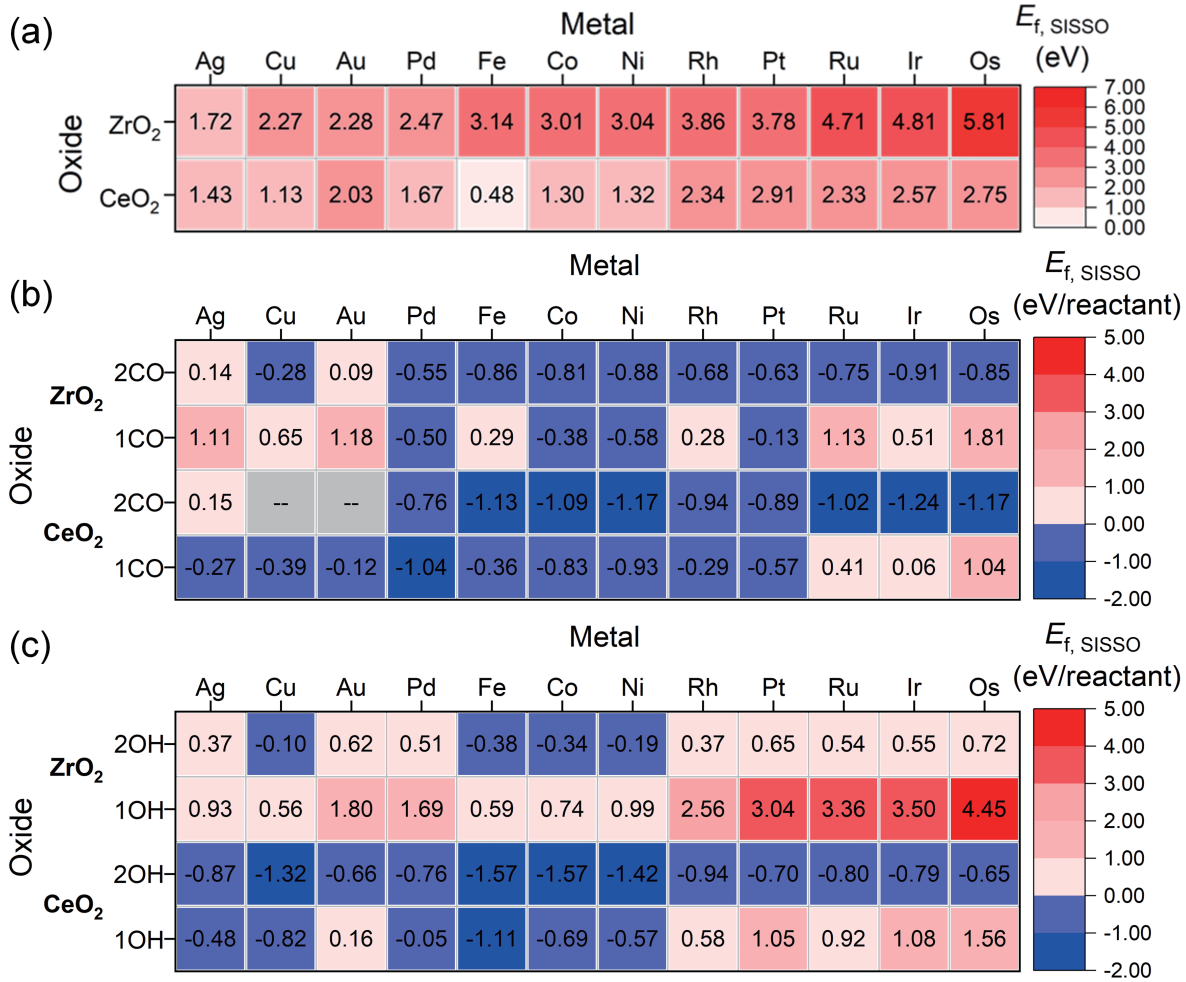

Fig. 7. Formation energies as predicted by Eq. (6) for (a) single metal atoms and Eq. (7) for (b) single-nucleus metal complexes with CO and (c) single-nucleus metal complexes with dissociated H_2O. These species are composed of metal atoms supported on ZrO_2 and CeO_2. From left to right, the $H_{sub,M}$ values of the metals increase sequentially, indicating that the metals become harder.

CSTR: 32290.14.JUSTC-2025-0010
DOI: 10.52396/JUSTC-2025-0010
JUSTC, **2026**, 55(X):

understand why the oxygen affinity of a metal atom on CeO_2 has a greater effect on the stability of SACs than does that on ZrO_2, we calculated the hydrogen adsorption energy on CeO_2, ZrO_2, TiO_2, and HfO_2 (Table 2) to evaluate the Lewis acidity of the lattice surface oxygen in the support, which reflects the ability to accept electrons from metal atoms.

Hydrogen adsorption on metal oxide surfaces is related to the Lewis acidity of surface oxygen, with a process involving electron transfer from H to surface oxygen[46]. Most metal elements, except Au, have electronegativity values comparable to or smaller than those of H (Table S5), resulting in an electronegativity difference between the metal atom and the oxygen atom that is similar to or greater than that between hydrogen and oxygen. A greater electronegativity difference typically leads to more ionic bonds between two atoms, which is associated with electron transfer processes. Therefore, the adsorption of a metal atom onto surface oxygen is also expected to correlate with the Lewis acidity of the oxygen atom. Our results show that a greater hydrogen adsorption energy (−1.16 and −3.13 eV for CeO_2 and TiO_2, respectively, in Table 2) correlates with a more negative value of c_2 (−0.42 and −0.23 for CeO_2 and TiO_2, respectively, in Table 1), indicating a promotional influence from the metal–oxygen interaction on E_f. In contrast, ZrO_2 and HfO_2 have positive hydrogen adsorption energies of 0.31 eV and positive c_2 values of approximately zero (0.12 in Table 1), indicating a slight inhibitory impact from metal–oxygen interactions. Hence, the impact of metal–support interactions is related to the Lewis acidity of the lattice oxygen in the support. CeO_2 and TiO_2 are characterized by greater Lewis acidity than ZrO_2 and HfO_2 are, leading to stronger promotional effects from metal–oxygen interactions.

In general, the hardness of a metal consistently influences the stability of SACs, whereas supports (such as CeO_2) with higher Lewis acidity can enhance the metal–support interaction, thereby further improving the stability of SACs. Overall, the Fe atoms on CeO_2, which combine relatively lower metal hardness with stronger metal–oxygen interactions, are the most easily dispersed, forming SACs with the lowest formation energy E_f.

3.3.3 Support-dependent adsorbate effects

The hardness and oxygen affinity of a metal influence the stability of SACs. However, under experimental conditions, the presence of reactants can further impact stability by binding to SACs to form single-nucleus metal complexes. To investigate this effect, we considered the presence of '1CO', '2CO', '1OH', and '2OH' in the systems shown in Fig. 7b and c and calculated the corresponding E_f values for single-nucleus metal complexes via Eq. (7). The DFT-calculated values, presented in Fig. S2, closely align with those obtained from Eq. (7). Additionally, the impact of CO and H_2O adsorption on E_f was examined by calculating the change in E_f (ΔE_f) from SACs to single-nucleus metal complexes.

First, we observed that the ΔE_f values for systems containing '1CO' and '1OH' are negative, as shown in Fig. 8a. Addi-

Table 2. Adsorption energy of hydrogen on different clean supports (unit: eV).

System	CeO_2	ZrO_2	TiO_2	HfO_2
E_{ads}	−1.16	+0.31	−3.13	+0.31

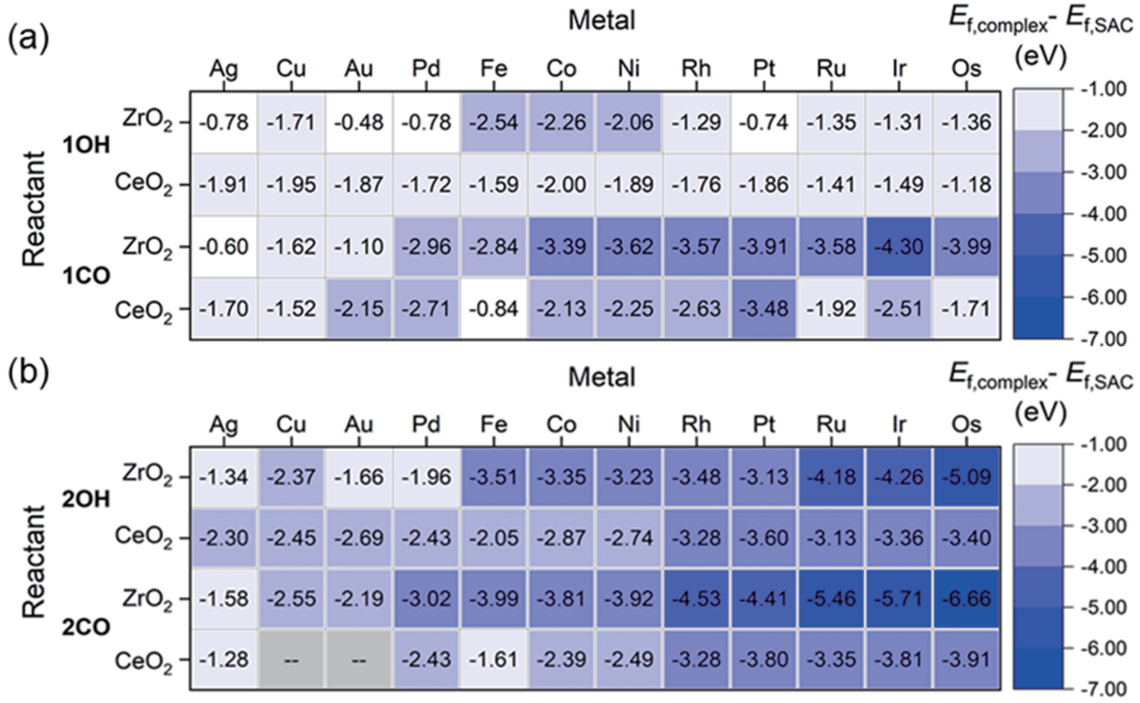

Fig. 8. Change in formation energy ($E_{f,complex}$−$E_{f,SAC}$, denoted ΔE_f) from single-metal atoms to single-nucleus metal complexes with CO and dissociative H_2O supported on ZrO_2 and CeO_2, as predicted by Eqs. (6) and (7). From left to right, the $H_{sub,M}$ values of the metals increase sequentially, indicating that the metals become harder.

CSTR: 32290.14.JUSTC-2025-0010
DOI: 10.52396/JUSTC-2025-0010
JUSTC, **2026**, 55(X):

tionally, the ΔE_f values for systems containing '2CO' and '2OH' are even more negative (Fig. 8b) because of the saturation of single metal atoms. Therefore, we focus primarily on the adsorption of CO and H_2O in systems with 2CO and 2OH (Fig. 8b), emphasizing how the support properties influence ΔE_f. This analysis involves comparing the ΔE_f values for metal atoms supported on CeO_2 and ZrO_2 in the presence of '2CO' or '2OH', establishing a correlation between the support properties and the impact of adsorbates on metal complex stability.

For identical single-nucleus metal complexes on different supports, only the coefficients c_i (c_1, c_2, c_3, and c_0 in Eq. (7)) vary, whereas the features Q_{MO}, Q_{MR}, and $H_{sub,M}$ remain constant, as shown in Table S1. Therefore, the variation in ΔE_f with changes in support is attributed primarily to the changes in c_i (Δc_i), which are denoted as Δc_1, Δc_2, and Δc_0 (Table 3). Notably, c_3 is exclusively present in Eq. (7) for single-nucleus metal complexes (Table 3). Δc_1, Δc_2, Δc_0 and c_3 represent the variation in the metal–support interaction, hydrogen adsorption (for dissociative H from H_2O), and metal–adsorbate interaction during CO or H_2O adsorption, respectively. Our analysis examined how these factors collectively influence ΔE_f (Fig. 8b), which can be expressed as $\Delta E_f = \Delta c_1 H_{sub,M} + \Delta c_2 Q_{mo} + c_3 Q_{mr} + \Delta c_0$. To identify the dominant factors, we compared the variations in Δc_1, Δc_2, Δc_0, and c_3 across different supports to determine which coefficients most significantly contributed to the observed changes in ΔE_f.

3.3.3.1 Impact of CO adsorption

First, the stabilizing effect of '2CO' on single-nucleus metal complexes is more pronounced for hard metals on ZrO_2 than on CeO_2, as evidenced by the more negative ΔE_f value (Fig. 8b). This difference arises primarily from enhanced metal–support interactions during CO adsorption, reflected by a negative Δc_2 (−0.31 in Table 3). In contrast, on CeO_2, Δc_2 becomes positive (0.18 in Table 3), suggesting that CO adsorption weakens the metal–support interaction, leading to the destabilization of single metal atoms.

While the values of Δc_1 (−0.59 and −0.26 for CeO_2 and ZrO_2, respectively), c_3 (−0.42 and −0.32 for CeO_2 and ZrO_2, respectively), and Δc_0 (0.07 and 0.28 for CeO_2 and ZrO_2, respectively) collectively result in a less negative ΔE_f for ZrO_2 than for CeO_2, the significantly greater negative Δc_2 on ZrO_2 outweighs these contributions. This highlights that the more pronounced reduction in ΔE_f caused by CO adsorption on ZrO_2 is driven primarily by the stronger metal–support interaction relative to CeO_2.

3.3.3.2 Impact of H_2O adsorption

The promotional effect of H_2O adsorption on E_f is influenced not only by the support but also by the metal species. For most hard metals, except Pd and Pt, the effect of '2OH' on ZrO_2 is more pronounced than that on CeO_2, as indicated by a more negative ΔE_f on ZrO_2 (Fig. 8b). In contrast, for Ag, Cu, Au, Pd, and Pt, this effect is more significant on CeO_2 (Fig. 8b). Therefore, we discuss these two groups of metals separately.

For most hard metals, excluding Pd and Pt, the promotional effect of '2OH' on E_f is more pronounced on ZrO_2 than on CeO_2, mirroring the trend observed with '2CO' (Fig. 8b). The negative Δc_2 value for ZrO_2 (−0.21 in Table 3) reflects an increase in metal–support interactions upon H_2O adsorption, contributing to the promotion effect. Conversely, the positive Δc_2 value for CeO_2 (0.34 in Table 3) suggests an inhibitory effect from these interactions.

A further comparison of Δc_1, Δc_0, and c_3 (Table 3) between the two supports revealed a similar trend to that observed with 2CO adsorption. These terms collectively contribute to a more positive ΔE_f on ZrO_2 than on CeO_2. However, this contribution is outweighed by the more negative Δc_2 for ZrO_2 (Table 3). Thus, the stronger enhancement of ΔE_f on ZrO_2 by '2OH' primarily arises from a more significant increase in the metal–support interaction due to H_2O adsorption, which is consistent with the conclusion drawn for '2CO'.

In contrast, for soft metals (Ag, Cu, and Au), as well as for Pd and Pt, the promotional effect of '2OH' on E_f on CeO_2 is more pronounced than that on ZrO_2, with ΔE_f values ranging from −2.30 eV to −3.60 eV (Fig. 8b). On ZrO_2, '2OH' has a less significant promotion effect, with ΔE_f values varying from −1.34 eV to −3.13 eV (Fig. 8b). This trend can be attributed to the smaller positive value of Δc_0 (0.20, Table 3) and the greater negative values of $\Delta c_1 H_{sub,M}$ (ranging from −1.98 to −3.94 eV, Table S8) on CeO_2 than on ZrO_2, where Δc_0 is 1.55 (Table 3), and $\Delta c_1 H_{sub,M}$ ranges from −0.59 to −1.18 eV (Table S8). Conversely, the Δc_2 and Δc_3 of CeO_2 (0.34, −0.56) are more positive than those of ZrO_2 (−0.21, −0.58), resulting in a more negative ΔE_f for ZrO_2. Therefore, the stronger promotional effect observed on CeO_2 is primarily a result of its more negative $\Delta c_1 H_{sub,M}$ and less positive Δc_0.

The $\Delta c_1 H_{sub,M}$ captures the effect of metal–support interactions on breaking metal–metal bonds within the metal bulk, where a more negative $\Delta c_1 H_{sub,M}$ indicates stronger metal–support interactions. Additionally, the coefficient Δc_0 is related to the hydrogen binding energy, as we considered the dissociative adsorption of H_2O. The hydrogen bonding energy is influenced by the Lewis acidity of the lattice oxygen in the support. The adsorption energy of hydrogen on CeO_2 is −1.16 eV, whereas on ZrO_2, it is 0.31 eV (Table 2), corresponding to Δc_0 values of 0.20 and 1.55 for CeO_2 and ZrO_2, respectively. This indicates that stronger hydrogen adsorption contributes to an energy gain for E_f on CeO_2, resulting in a less positive Δc_0. Therefore, both the metal–support interac-

Table 3. The difference between the coefficients (Δc_i) of complex and SACs.

System	Δc_1	Δc_2	c_3	Δc_0
2CO-M/CeO_2	−0.59	0.18	−0.42	0.07
2CO-M/ZrO_2	−0.26	−0.31	−0.32	0.28
2OH-M/CeO_2	−0.67	0.34	−0.56	0.20
2OH-M/ZrO_2	−0.20	−0.21	−0.58	1.55

CSTR: 32290.14.JUSTC-2025-0010
DOI: 10.52396/JUSTC-2025-0010
JUSTC, **2026**, 55(X):

tions and the hydrogen adsorption strength of the support play a role in influencing the effect of '2OH'.

Overall, the support influences not only the stability of single-nucleus metal complexes with CO but also that with OH through H adsorption or metal–support interactions. Since the support primarily affects metal–support interactions via the Lewis acidity of surface oxygen atoms, the Lewis acidity of surface oxygen is expected to play a key role in affecting ΔE_f. Supports with a lower Lewis acidity of surface oxygen (ZrO_2) enhance metal–support interactions, leading to a greater promotional effect from CO on all metals and from H_2O on complexes primarily composed of hard metals. Conversely, supports with a relatively high Lewis acidity of surface oxygen in CeO_2 facilitate hydrogen adsorption, resulting in a promotional effect from H_2O on complexes formed by the soft metals Pd and Pt.

Frenkel et al. used in situ TEM to observe the reversible disappearance and reappearance of perimeter Pt atoms on Pt/CeO_2 under WGS conditions. CO-DRIFTS detected CO adsorption features on low-coordinated Pt atoms at 180 °C, indicating that single Pt atom complexes with CO[47]. Similarly, $Rh_1(CO)_2$ forms on CeO_2 in a pure CO atmosphere[9], supporting the transition from positive E_f for isolated Pt and Rh atoms to negative E_f for single-nucleus complexes in Fig. 7 when CO is present. While direct evidence for metal complex formation with H_2O remains elusive, in situ analyses suggest that hydroxyl groups from dissociated water enhance the dispersion of metal atoms (e.g., Ag, Cu, Pd, and Pt)[16–18]. This implies that H_2O can potentially contribute to single-nucleus complex formation, as reflected in the more negative E_f for complexes involving OH than for those involving isolated metal atoms, as shown in Fig. 7.

3.4 Nanoparticle dissociation vs. Ostwald ripening

Next, we evaluated the influence of reaction conditions on the stability of single-nucleus metal complexes under relatively low partial pressures of CO and H_2O (set to 0.1 mbar) at 300 K, with corresponding chemical potentials of −0.63 eV and −0.16 eV, respectively. After collecting the dataset of G_f for single-nucleus metal complexes across various metals on CeO_2 and ZrO_2, we analyzed the trends of NP dissociation into single-atom complexes and Ostwald ripening (OR), which depend on the sign of the G_f for single-nucleus metal complexes. Specifically, when the G_f values are positive, the OR process occurs, whereas a negative G_f indicates that single-nucleus metal complexes are more stable than NPs are, driving the dissociation of NPs into single-nucleus metal complexes[48].

Under a CO atmosphere ('2CO' in Fig. 9a), the dissociation of NPs is more pronounced for most hard metals on ZrO_2 with a negative G_f, except for Pd and Pt, where soft metals exhibit a stronger tendency for the OR process with a positive G_f. On CeO_2, the OR process is observed exclusively for soft metals, whereas the dissociation of NPs into single-nucleus metal complexes is more prevalent for the remaining hard metals. In general, under CO conditions, hard metals on both CeO_2 and ZrO_2 generally exhibit a stronger tendency for NP dissociation, whereas the OR process is typically favored by soft metals. This is because, with increasing metal hardness, the interactions between the metal and oxygen (Q_{MO}) as well as between the metal and CO (Q_{MR}) are enhanced (Table S1), resulting in a more negative E_f.

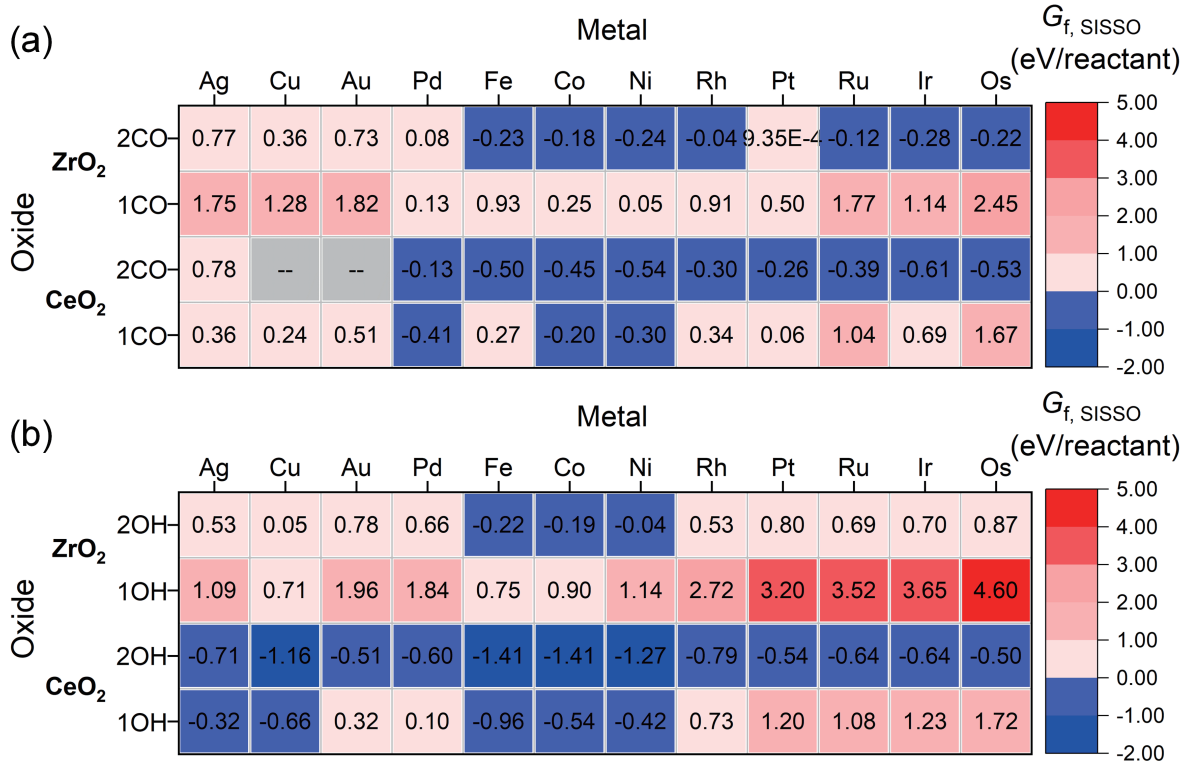

Fig. 9. Formation free energies of single-nucleus metal complexes with (a) CO and (b) dissociative H_2O, which are composed of metal atoms supported on ZrO_2 and CeO_2. The partial pressures of CO and H_2O are set to 0.1 mbar each at 300 K.

CSTR: 32290.14.JUSTC-2025-0010
DOI: 10.52396/JUSTC-2025-0010
JUSTC, **2026**, 55(X):

Under a H_2O atmosphere ('2OH' in Fig. 9b), unlike under CO conditions, the OR process occurs exclusively on ZrO_2 for all metals except Fe, Co, and Ni, whose NPs tend to dissociate into single-nucleus metal complexes. On CeO_2, H_2O induces the dissociation of all the metal species from the NPs. Therefore, in the case of '2OH', the support effect is more pronounced. This is attributed to the strong Lewis acidity of the lattice oxygen on the CeO_2 surface, which facilitates the adsorption of dissociated hydrogen from H_2O and enhances the metal–support interactions, thereby promoting the stabilization of H_2O on the SAC.

In general, supports with lattice oxygen and stronger Lewis acidity (such as CeO_2), combined with metals of higher hardness, promote a greater tendency for NP dissociation, whereas the opposite favors the OR process. Additionally, CO has a stronger preference for promoting NP dissociation, whereas higher pressure is required for H_2O to shift the process from OR to NP dissociation on a support with weaker Lewis acidity (such as ZrO_2).

4 Conclusions

The structure of supported transition metal catalysts can change in the presence of reactants under experimental conditions, leading to the formation of dispersed metal species that bind to ligands from reactants, forming single-nucleus metal complexes. Understanding the stability of these single-nucleus metal complexes is crucial for determining the active configurations of catalysts under experimental conditions. In our study, we employed multitask regression to identify descriptors for the formation energy of single-nucleus metal complexes in the presence of common reactants (CO and H_2O). This approach incorporates key factors, including the hardness of the metal, metal–support interactions, and adsorbate–metal interactions. Our findings reveal that changes in metal species primarily impact the stability of single-nucleus metal complexes via the hardness of the metal and the strength of the metal–adsorbate interaction, which is further modulated by the Lewis acidity of the lattice oxygen in the support. However, the influence of metal–support interactions can become more pronounced when the support and adsorbates are varied.

For supports with weaker Lewis acidity, such as ZrO_2, CO exerts a more significant promotional effect through enhanced metal–support interactions ($\Delta c_2 Q_{MO}$), thereby increasing the stability of single-nucleus metal complexes compared with that of supports such as CeO_2. In contrast, the stability of OH-containing single-nucleus metal complexes depends on both the metal and the support. For most hard metals, metal–support interactions ($\Delta c_2 Q_{MO}$) have a substantial promotional effect on supports with weaker Lewis acidity. However, for soft metals (Ag, Cu, and Au), as well as Pd and Pt, stronger hydrogen adsorption on supports with higher Lewis acidity enhances the stability of single-nucleus metal complexes.

The tendency of the NPs to dissociate into single-nucleus metal complexes or ORs was evaluated on the basis of the free formation energy G_f under experimental conditions. Under a CO atmosphere, the sign of G_f is more closely related to the hardness of the metal. For both CeO_2 and ZrO_2, as the metal hardness increases, the interactions between the metal and oxygen are enhanced in SACs. Hence, hard metals exhibit a stronger tendency for NP dissociation, whereas soft metals (Ag, Cu, and Au) are more inclined toward the OR process. Under a H_2O atmosphere, this tendency is influenced by the partial pressure of H_2O. At low pressure, the stability of single-nucleus metal complexes is comparable to that of SACs. Supports with higher Lewis acidity, such as CeO_2, enhance metal–support interactions, thereby promoting the dissociation of NPs. However, under relatively high partial pressures, the increased promotion effect of CO adsorption on ZrO_2 can further drive NP dissociation. In general, the tendency of NPs to dissociate into single-nucleus metal complexes or undergo OR depends on the metal hardness, type of support, and reaction conditions, as described by Eq. (7).

To identify a descriptor for single-nucleus metal complexes with a single ligand type, data-driven machine learning techniques can be further applied to develop descriptors for complexes with multiple ligands. For reactions such as water–gas shifts, this approach can be extended to systems where Pt binds both OH and CO. We also recommend in situ studies under CO- or H_2O-rich conditions to validate these predictions and enhance our understanding of metal complex formation.

Acknowledgements

This work was supported by the Key Technologies R&D Program of China (2021YFA1502804), the Strategic Priority Research Program of the Chinese Academy of Science (XDB0450102), the National Natural Science Foundation of China (22172150, 22221003, 22222306), the Innovation Program for Quantum Science and Technology (2021ZD0303302), and high-performance computational resources provided by the University of Science and Technology of China and the Hefei Advanced Computing Center.

Conflict of interest

The authors declare that they have no conflict of interest.

References

[1] Ogo S, Sekine Y. Recent progress in ethanol steam reforming using non-noble transition metal catalysts: A review. *Fuel Processing Technology,*, **2020**, *199*: 106238.
[2] Zhang H, Sun Z, Hu Y H. Steam reforming of methane: Current states of catalyst design and process upgrading. *Renewable and Sustainable Energy Reviews,*, **2021**, *149*: 111330.
[3] Gänzler A M, Casapu M, Vernoux P, et al. Tuning the structure of platinum particles on ceria in situ for enhancing the catalytic performance of exhaust gas catalysts. *Angewandte Chemie International Edition,*, **2017**, *56* (42): 13078–13082.
[4] Wu D F, Liu S X, Zhong M Q, et al. Nature and dynamic evolution of Rh single atoms trapped by CeO2 in CO hydrogenation. *ACS Catalysis*, **2022**, *12* (19): 12253–12267.
[5] Muravev V, Spezzati G, Su Y Q, et al. Interface dynamics of Pd–CeO2 single-atom catalysts during CO oxidation. *Nature Catalysis*, **2021**, *4*: 469–478.
[6] Fierro-Gonzalez J C, Kuba S, Hao Y, et al. Oxide- and zeolite-supported molecular metal complexes and clusters: physical characterization and determination of structure, bonding, and metal

CSTR: 32290.14.JUSTC-2025-0010
DOI: 10.52396/JUSTC-2025-0010
JUSTC, **2026**, 55(X):

oxidation state. *The Journal of Physical Chemistry B*, **2006**, *110* (27): 13326–13351.
[7] Lu Y, Zhou S, Kuo C T, et al. Unraveling the intermediate reaction complexes and critical role of support-derived oxygen atoms in CO oxidation on single-atom Pt/CeO_2. *ACS Catalysis*, **2021**, *11* (14): 8701–8715.
[8] Yan G, Tang Y, Li Y, et al. Reaction product-driven restructuring and assisted stabilization of a highly dispersed Rh-on-ceria catalyst. *Nature Catalysis*, **2022**, *5* (2): 119–127.
[9] Wu D F, Zhou S Y, Du C C, et al. The proximity between hydroxyl and single atom determines the catalytic reactivity of Rh_1/CeO_2 single-atom catalysts. *Nano Research*, **2024**, *17* (1): 397–406.
[10] Roiaz M, Falivene L, Rameshan C, et al. Roughening of copper (100) at elevated CO pressure: Cu adatom and cluster formation enable CO dissociation. *The Journal of Physical Chemistry C*, **2019**, *123* (13): 8112–8121.
[11] Eren B, Zherebetskyy D, Patera L L, et al. Activation of Cu(111) surface by decomposition into nanoclusters driven by CO adsorption. *Science*, **2016**, *351* (6272): 475–478.
[12] Tao F, Dag S, Wang L W, et al. Break-up of stepped platinum catalyst surfaces by high CO coverage. *Science*, **2010**, *327* (5967): 850–853.
[13] Dvořák F, Farnesi Camellone M, Tovt A, et al. Creating single-atom Pt-ceria catalysts by surface step decoration. *Nature Communications*, **2016**, *7* (1): 10801.
[14] Nie L, Mei D, Xiong H, et al. Activation of surface lattice oxygen in single-atom Pt/CeO_2 for low-temperature CO oxidation. *Science*, **2017**, *358* (6369): 1419–1423.
[15] Fan Y M, Wang F, Li R T, et al. Surface hydroxyl-determined migration and anchoring of silver on alumina in oxidative redispersion. *ACS Catalysis*, **2023**, *13* (4): 2277–2285.
[16] Fan Y M, Li R T, Wang B B, et al. Water-assisted oxidative redispersion of Cu particles through formation of Cu hydroxide at room temperature. *Nature Communications*, **2024**, *15*: 3046.
[17] Sun Y N, Zhang J F, Zhou D D, et al. Tailoring the dispersion of metals on ZnO with preadsorbed water. *The Journal of Physical Chemistry Letters*, **2022**, *13* (43): 10207–10215.
[18] Wang F, Li, K, Li B L, et al. Identification of direct anchoring sites for monoatomic dispersion of precious metals (Pt, Pd, Ag) on CeO_2 support. *Angewandte Chemie International Edition,*, **2024**, *63* (11): e202318492.
[19] Tan K, Dixit M, Dean J, et al. Predicting metal–support interactions in oxide-supported single-atom catalysts. *Industrial & Engineering Chemistry Research*, **2019**, *58* (44): 20236–20246.
[20] Wang Y W, Song E H, Qiu W J, et al. Recent progress in theoretical and computational investigations of structural stability and activity of single-atom electrocatalysts. *Progress in Natural Science: Materials International,*, **2019**, *29* (3): 256–264.
[21] Yu Z R, Xu H X, Cheng D J. Design of single atom catalysts. *Advances in Physics: X*, **2021**, *6* (1): 1905545.
[22] O'Connor N J, Jonayat A S M, Janik M J, et al. Interaction trends between single metal atoms and oxide supports identified with density functional theory and statistical learning. *Nature Catalysis*, **2018**, *1*: 531–539.
[23] Mao Z, Campbell C T. Predicting a key catalyst-performance descriptor for supported metal nanoparticles: metal chemical potential. *ACS Catalysis*, **2021**, *11* (13): 8284–8291.
[24] Wang T R, Hu J Y, Ouyang R H, et al. Nature of metal-support interaction for metal catalysts on oxide supports. *Science*, **2024**, *386* (6724): 915–920.
[25] Wang Y, Wagner N, Rondinelli J M. Symbolic regression in materials science. *MRS Communications*, **2019**, *9*: 793–805.
[26] Ouyang R H, Curtarolo S, Ahmetcik E, et al. SISSO: A compressed-sensing method for identifying the best low-dimensional descriptor in an immensity of offered candidates. *Physical Review Materials*, **2018**, *2*: 083802.
[27] Ouyang R H, Ahmetcik E, Carbogno C, et al. Simultaneous learning of several materials properties from incomplete databases with multi-task SISSO. *Journal of Physics: Materials*, **2019**, *2* (2): 024002.
[28] Farid B, Godby R W. Cohesive energies of crystals. *Physical Review B*, **1991**, *43* (17): 14248–14250.
[29] Kresse G, Furthmüller J. Efficient iterative schemes for ab initio total-energy calculations using a plane-wave basis set. *Physical Review B*, **1996**, *54* (16): 11169–11186.
[30] Kresse G, Furthmüller J. Efficiency of ab-initio total energy calculations for metals and semiconductors using a plane-wave basis set. *Computational Materials Science,*, **1996**, *6* (1): 15–50.
[31] Perdew J P, Burke K, Ernzerhof M. Generalized gradient approximation made simple. *Physical Review Letters*, **1996**, *77* (18): 3865–3868.
[32] Kresse G, Joubert D. From ultrasoft pseudopotentials to the projector augmented-wave method. *Physical Review B*, **1999**, *59* (3): 1758–1775.
[33] Blöchl P E. Projector augmented-wave method. *Physical Review B*, **1994**, *50* (24): 17953–17979.
[34] Dudarev S L, Botton G A, Savrasov S Y, et al. Electron-energy-loss spectra and the structural stability of nickel oxide: An LSDA+U study. *Physical Review B*, **1998**, *57* (3): 1505–1509.
[35] Loschen C, Carrasco J, Neyman K M, et al. First-principles LDA+U and GGA+U study of cerium oxides: Dependence on the effective U parameter. *Physical Review B*, **2007**, *75* (3): 035115.
[36] Fabris S, de Gironcoli S, Baroni S, et al. Taming multiple valency with density functionals: A case study of defective ceria. *Physical Review B*, **2005**, *71* (4): 041102.
[37] Huang M, Fabris S. CO adsorption and oxidation on ceria surfaces from DFT+U calculations. *The Journal of Physical Chemistry C*, **2008**, *112* (23): 8643–8648.
[38] Hu Z, Metiu H. Choice of *U* for DFT+*U* calculations for titanium oxides. *The Journal of Physical Chemistry C*, **2011**, *115* (13): 5841–5845.
[39] Monkhorst H J, Pack J D. Special points for Brillouin-zone integrations. *Physical Review B*, **1976**, *13* (12): 5188–5192.
[40] Gerward L, Staun Olsen J, Petit L, et al. Bulk modulus of CeO_2 and PrO_2—An experimental and theoretical study. *Journal of Alloys and Compounds,*, **2005**, *400*: 56–61.
[41] Song W, Hensen E J M. Structure sensitivity in CO oxidation by a single Au atom supported on ceria. *The Journal of Physical Chemistry C*, **2013**, *117* (15): 7721–7726.
[42] Tian D, Zeng C H, Wang H, et al. Effect of transition metal Fe adsorption on CeO_2(110) surface in the methane activation and oxygen vacancy formation: A density functional theory study. *Applied Surface Science,*, **2017**, *416*: 547–564.
[43] Ha M, Kim D Y, Umer M, et al. Tuning metal single atoms embedded in N_xC_y moieties toward high-performance electrocatalysis. *Energy & Environmental Science*, **2021**, *14* (6): 3455–3468.
[44] Hu S L, Li W X. Sabatier principle of metal-support interaction for design of ultrastable metal nanocatalysts. *Science*, **2021**, *374* (6573): 1360–1365.
[45] Cao S Y, Hu S L, Li W X. First-principles thermodynamics study of CO/OH induced disintegration of precious metal nanoparticles on TiO_2(110). *Chinese Journal of Chemical Physics*, **2023**, *36* (4): 411–418.
[46] Li M, Sakong S, Groß A. In search of the active sites for the selective catalytic reduction on tungsten-doped vanadia monolayer catalysts supported by TiO_2. *ACS Catalysis*, **2021**, *11* (12): 7411–7421.
[47] Li Y, Kottwitz M, Vincent J L, et al. Dynamic structure of active sites in ceria-supported Pt catalysts for the water gas shift reaction. *Nature Communications*, **2021**, *12* (1): 914.
[48] Ouyang R H, Liu J X, Li W X. Atomistic Theory of Ostwald ripening and disintegration of supported metal particles under reaction conditions. *Journal of the American Chemical Society*, **2013**, *135* (5): 1760–1771.

CSTR: 32290.14.JUSTC-2025-0010
DOI: 10.52396/JUSTC-2025-0010
JUSTC, **2026**, 55(X):